




Cite this: *Phys. Chem. Chem. Phys.*,  
2024, 26, 12957

# Does the active hydrogen atom in the hydantoin anion affect the physical properties, CO<sub>2</sub> capture and conversion of ionic liquids?†

Tingting Chen,<sup>a</sup> Zhongyuan Sun,<sup>a</sup> Yujun Guo<sup>a</sup> and Yingjie Xu  <sup>\*,ab</sup>

Compared to the effect of the active hydrogen atom in the cation in protic ionic liquids (ILs) on their properties and applications, there are very few reports on the role of the active hydrogen atom in the anion. In order to better understand the role of the active hydrogen atom in the anion, the physical properties, CO<sub>2</sub> capture and conversion of three hydantoin-based anion-functionalized ILs ([P<sub>4442</sub>][Hy], [P<sub>4442</sub>]<sub>2</sub>[Hy], and [HDBU][Hy]) have been investigated via experiments, spectroscopy, and DFT calculations in this work. The results show that the active hydrogen atom in the anion can form anionic hydrogen bonding networks, which significantly increase the melting point and viscosity and decrease the basicity of the IL, thereby weakening its ability to capture and convert CO<sub>2</sub>. Interestingly, [P<sub>4442</sub>][Hy] undergoes a solid/liquid two-phase transition during CO<sub>2</sub> absorption/desorption due to the formation of quasi-intramolecular hydrogen bonding between the active hydrogen atom and the O<sup>−</sup> atom of the absorbed CO<sub>2</sub>, suggesting that the presence of the active hydrogen atom gives [P<sub>4442</sub>][Hy] the potential to be an excellent molecular switch. As there is no active hydrogen atom in the anion of [P<sub>4442</sub>]<sub>2</sub>[Hy], it shows excellent CO<sub>2</sub> capture and conversion performance through the double-site interaction. [HDBU][Hy] shows the weakest catalytic CO<sub>2</sub> conversion due to the presence of active hydrogen atoms on both its anion and cation. Therefore, the active hydrogen atom in the anion may play a more important role in the properties and potential applications of ILs than the active hydrogen atom in the cation.

Received 7th December 2023,  
Accepted 7th April 2024

DOI: 10.1039/d3cp05965k

rsc.li/pccp

## 1. Introduction

Ionic liquids (ILs) are promising neoteric materials composed only of anions and cations with unique physical properties. They have a wide range of potential applications, and are classified as aprotic ILs (APILs) and protic ILs (PILs).<sup>1–5</sup> Among them, PILs are formed by the transfer of a proton from a Brønsted acid to a Brønsted base,<sup>1</sup> so they have an active hydrogen atom in the cation, which allows the formation of strong intermolecular hydrogen bonds with the anion, resulting in higher viscosity ( $\eta$ ), lower molar volume, and lower enthalpy of vaporization than those of APILs.<sup>1</sup> Consequently, the effects of the active hydrogen atom of PILs on CO<sub>2</sub> capture and catalytic properties have attracted considerable attention. As reported by Wang *et al.*,<sup>5,6</sup> both the [HMTBD][Im] PIL and

the [P<sub>66614</sub>][Im] APIL achieved equimolar CO<sub>2</sub> absorption through the chemical interaction of [Im]<sup>−</sup> with CO<sub>2</sub>, but the former had a relatively slower absorption rate and a significant increase in  $\eta$  after CO<sub>2</sub> absorption. Similar results were found for other azole-based anionic PILs and APILs, suggesting that the active hydrogen atom in the cation of PILs hardly affects the basicity, but their  $\eta$  generally increases with CO<sub>2</sub> uptake.<sup>7–9</sup> Subsequent theoretical studies have shown that the O<sup>−</sup> in the [anion-CO<sub>2</sub>]<sup>−</sup> intermediate produced by PILs during CO<sub>2</sub> uptake can form intermolecular hydrogen bonds with the active hydrogen atom in the cation, leading to an increase in  $\eta$  and hindering CO<sub>2</sub> mass transfer.<sup>10–13</sup> Nevertheless, there is still some controversy about the role of the active hydrogen atom in the cation of PILs in catalyzing CO<sub>2</sub> conversion.<sup>14–20</sup> For example, Liu *et al.*<sup>14</sup> and Mu *et al.*<sup>15</sup> proposed that the catalytic performance of the [HDBU][TFE] PIL for the reaction of CO<sub>2</sub> with 2-aminobenzonitrile was superior to that of the [EtDBU][TFE] APIL, which was attributed to the activation of the −CN of the substrate by the active hydrogen atom in [HDBU]<sup>+</sup> of [HDBU][TFE] through hydrogen bond interaction. However, Zhang *et al.*<sup>16</sup> reported that the catalytic ability of [HDBU][Suc] and [HTMG][Suc] PILs was lower than that of the [BzTMA][Suc]

<sup>a</sup> Department of Chemistry, Shaoxing University, 508 Huancheng West Road, Shaoxing, Zhejiang Province, 312000, China. E-mail: xuyj@usx.edu.cn

<sup>b</sup> Zhejiang Engineering Research Center of Fat-soluble Vitamin, 508 Huancheng West Road, Shaoxing, Zhejiang Province, 312000, China

† Electronic supplementary information (ESI) available. See DOI: <https://doi.org/10.1039/d3cp05965k>

APIL, which was attributed to the fact that the active hydrogen atom in the cation could enhance anion–cation interactions thereby weakening the CO<sub>2</sub> capture capacity of [Suc]<sup>−</sup>. Therefore, the active hydrogen atom in the cation of PILs is crucial for their physical properties and applications.

In fact, in addition to the presence of active hydrogen atoms in the cation of PILs, active hydrogen atoms may also be present in the anion of some APILs. For example, when a dibasic acid is neutralized with equimolar alkylphosphonium hydroxide, an active hydrogen atom is present in the anion of an APIL. As the position of the active hydrogen atom in the APIL is different from that of the PIL, the effects on the respective properties may be different. Compared with the study of the effect of the active hydrogen atom in the cation of a PIL on its properties and applications,<sup>10–13</sup> few reports have discussed the role of the active hydrogen atom in the anion of an APIL. Therefore, it is worthwhile to study the role of the active hydrogen atom in the anion and to reveal the similarities and differences between the active hydrogen atom in the anion of an APIL and that in the cation of a PIL.

To this end, a novel APIL with the active hydrogen atom in the anion, [P<sub>4442</sub>][Hy], is prepared *via* a neutralization reaction of [P<sub>4442</sub>][OH] with equimolar amounts of hydantoin (Scheme 1). For comparison, [P<sub>4442</sub>]<sub>2</sub>[Hy] without the active hydrogen atom and [HDBU][Hy] with the active hydrogen atoms in both the anion and cation are also synthesized (Scheme 1).  $\eta$  and basicity of three hydantoin-based ILs are determined to study the effect of the active hydrogen atom in the anion on their physical properties. The CO<sub>2</sub> absorption behavior and absorption mechanism of [P<sub>4442</sub>][Hy] and [P<sub>4442</sub>]<sub>2</sub>[Hy] are investigated to explore the role of the active hydrogen atom in the anion on CO<sub>2</sub> capture and activation. Moreover, the reaction of CO<sub>2</sub> with 2-aminobenzonitrile catalyzed by hydantoin-based ILs is used as an example to investigate the effect of the active hydrogen atom in the anion on the catalytic conversion of CO<sub>2</sub>. Based on the physical properties, CO<sub>2</sub> absorption and catalytic reaction

experiments, spectra, and DFT calculations, it is found that the active hydrogen atom in the hydantoin-based anion can form anionic hydrogen bonding networks, which significantly increase  $\eta$  and decrease the basicity of the IL thereby weakening its ability to capture and convert CO<sub>2</sub>. Interestingly, the active hydrogen atom in the anion allows [P<sub>4442</sub>][Hy] to be a potential CO<sub>2</sub>-response molecular switch. [P<sub>4442</sub>]<sub>2</sub>[Hy] with no active hydrogen atom showing excellent CO<sub>2</sub> capture and conversion ability through the double-site interaction. The present work suggests that the active hydrogen atom in the anion may play a more important role in the properties and applications of the IL than the active hydrogen atom in the cation.

## 2. Experimental and theoretical

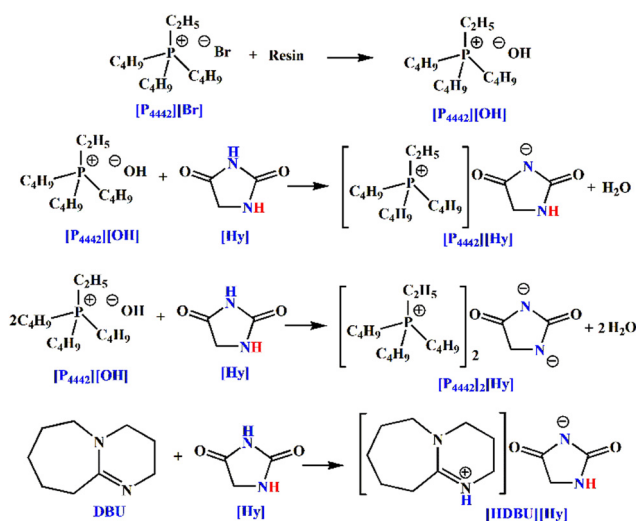
### Materials

Hydantoin (Hy, >99%), 1,8-diazabicyclo[5.4.0]undec-7-ene (DBU, >98%), tributylphosphine (P<sub>444</sub>, >95%), bromoethane (C<sub>2</sub>H<sub>5</sub>Br, >99%), sodium hydroxide (NaOH, >99%), acetonitrile (CH<sub>3</sub>CN, >98%), ethanol (>99%), 2-aminobenzonitrile (C<sub>7</sub>H<sub>6</sub>N<sub>2</sub>, >99%), potassium hydrogen phthalate (C<sub>8</sub>H<sub>5</sub>O<sub>4</sub>K, 99.99%), and a basic anion-exchange resin (Amberlite 717, AR) were purchased from Aladdin Reagent Co. Ltd, Shanghai, China. CO<sub>2</sub> (>99.9%) and N<sub>2</sub> (>99.999%) were purchased from Shaoxing Zhongxu Gas Factory. All chemicals were used as received and obtained in highest purity grade possible.

### Synthesis and characterization of hydantoin-based ILs

The synthesis process of [P<sub>4442</sub>][Hy] and [P<sub>4442</sub>]<sub>2</sub>[Hy] is similar to that in our previous work.<sup>21,22</sup> First, P<sub>444</sub> and C<sub>2</sub>H<sub>5</sub>Br were reacted under N<sub>2</sub> protection to give the tributylethylphosphonium bromide ([P<sub>4442</sub>][Br]). Second, [P<sub>4442</sub>][Br] was passed through the basic anion-exchange resin activated by NaOH to give the tributylethylphosphonium hydroxide ([P<sub>4442</sub>][OH]) ethanol solution, and its concentration was determined by titration of a potassium hydrogen phthalate solution. Finally, [P<sub>4442</sub>][Hy] was prepared by neutralization reaction of [P<sub>4442</sub>][OH] and Hy in a molar ratio of 1:1 for 48 h at room temperature. [P<sub>4442</sub>]<sub>2</sub>[Hy] was synthesized similarly by neutralization of [P<sub>4442</sub>][OH] with Hy in a 2:1 molar ratio. A large amount of ethanol and a small amount of water were removed from the [P<sub>4442</sub>][Hy] and [P<sub>4442</sub>]<sub>2</sub>[Hy] under vacuum at 343.15 K. Trace amounts of water were removed from [P<sub>4442</sub>][Hy] and [P<sub>4442</sub>]<sub>2</sub>[Hy] with a freeze dryer for 72 h. [HDBU][Hy] was synthesized by the equimolar proton transfer reaction of Hy with DBU, similar to the preparation of [HDBU][Im] and [HTMG][Im].<sup>7,8</sup> In a typical synthesis of [HDBU][Hy], 0.25 mol Hy was divided into several parts and added into 0.25 mol DBU in batches under vigorous stirring at 353.15 K for 24 h. The obtained IL was then dried under vacuum at 353.15 K for at least 48 h to remove possible traces of water. The specific reaction equations are shown in Scheme 1.

The water content of [P<sub>4442</sub>][Hy], [P<sub>4442</sub>]<sub>2</sub>[Hy], and [HDBU][Hy] was determined *via* Karl Fisher Coulometric Titration (Mettler Toledo C20S), and was found to be 820, 860, and 1000 ppm,



Scheme 1 Synthesis of [P<sub>4442</sub>][Hy], [P<sub>4442</sub>]<sub>2</sub>[Hy], and [HDBU][Hy].

respectively. The structure of  $[P_{4442}][Hy]$ ,  $[P_{4442}]_2[Hy]$ , and  $[HDBU][Hy]$  was characterized by  $^1H$  NMR spectroscopy using a Bruker AVANCE III 400 MHz spectrometer. The thermal stability of  $[P_{4442}][Hy]$ ,  $[P_{4442}]_2[Hy]$ ,  $[HDBU][Hy]$ ,  $[P_{4442}][Hy-CO_2]$ , and  $[P_{4442}]_2[Hy-2CO_2]$  was determined by measuring their thermogravimetric analysis (TGA) curves under  $N_2$  of  $60\text{ mL min}^{-1}$  at  $10\text{ }^\circ\text{C min}^{-1}$ . The melting point of  $[P_{4442}][Hy]$  and  $[HDBU][Hy]$  was determined by differential scanning calorimetry (Mettler Toledo DSC1) at  $15\text{ }^\circ\text{C min}^{-1}$ .

#### Measurement of $\eta$ of $[P_{4442}][Hy]$ , $[P_{4442}][Hy-CO_2]$ , and $[P_{4442}]_2[Hy]$

$\eta$  of  $[P_{4442}]_2[Hy]$  was measured using an Anton Paar AMVn falling ball automated microviscometer. The measurement methods and procedures were described in our previous work.<sup>21</sup> The temperature for  $\eta$  measurement was controlled with a built-in precise Peltier thermostat with an accuracy of  $T = \pm 0.05\text{ K}$ .  $\eta$  of  $[P_{4442}][Hy]$  and  $[P_{4442}][Hy-CO_2]$  was measured with a Brookfield DV2T viscometer,<sup>23</sup> and the temperature was controlled using a super-thermostatic water bath with an accuracy of  $T = \pm 0.05\text{ K}$ .

#### Measurement of the basicity of hydantoin-based ILs

The basicity of  $[P_{4442}][Hy]$ ,  $[P_{4442}]_2[Hy]$ , and  $[HDBU][Hy]$  are characterized using pyrrole as a probe molecule.<sup>24,25</sup> FT-IR spectra of the mixtures of IL with equimolar pyrrole were measured by using a Nicolet 6700 Fourier transform infrared spectrometer equipped with a DTGS detector, KBr windows, and ATR accessory. Each ATR-IR spectrum was recorded with a resolution of  $2\text{ cm}^{-1}$  and 16 parallel scans, and the wavenumber was in the range from  $4000$  to  $600\text{ cm}^{-1}$ . The basicity of the hydantoin-based ILs was characterized by comparing the changes of the N-H infrared stretching vibrations of pure pyrrole and pyrrole in the mixture.

#### $CO_2$ absorption/desorption and absorption mechanism by $[P_{4442}][Hy]$ and $[P_{4442}]_2[Hy]$

The process of  $CO_2$  absorption and desorption by  $[P_{4442}][Hy]$  and  $[P_{4442}]_2[Hy]$  was similar to that in our previous work.<sup>21</sup> A typical process is as follows:  $0.1\text{ MPa } CO_2$  was bubbled through approximately  $1.0\text{ g}$  IL in a glass container with an inner diameter of  $10\text{ mm}$ , and the flow rate was controlled at about  $60\text{ mL min}^{-1}$ . The glass container was placed in a thermostat at the desired temperature, and the amount of  $CO_2$  absorbed was measured periodically using an analytical balance with an accuracy of  $\pm 0.0001\text{ g}$  until the weight was constant. Low partial pressure  $CO_2$  was diluted with  $N_2$  by controlling the flow rate ratio. Desorption was carried out at  $343.15\text{ K}$  by bubbling  $N_2$  at a flow rate of about  $20\text{ mL min}^{-1}$  through the  $CO_2$ -absorbed  $[P_{4442}][Hy]$  and  $CO_2$ -absorbed  $[P_{4442}]_2[Hy]$ , and the obtained  $[P_{4442}][Hy]$  and  $[P_{4442}]_2[Hy]$  were used for the next capture of  $CO_2$ . The  $CO_2$  absorption mechanism of  $[P_{4442}][Hy]$  and  $[P_{4442}]_2[Hy]$  was studied by comparing the FT-IR and  $^{13}C$  NMR spectra of  $CO_2$ -free and  $CO_2$ -absorbed ILs. FT-IR spectra were recorded on a Nicolet 6700 Fourier transform infrared spectrometer with an ATR accessory.

#### Reaction of $CO_2$ with 2-aminobenzonitrile to prepare quinazoline-2,4(1*H*,3*H*)-diones catalyzed by hydantoin-based ILs

The catalytic properties of  $[P_{4442}][Hy]$ ,  $[P_{4442}]_2[Hy]$ , and  $[HDBU][Hy]$  for the reaction of  $CO_2$  with 2-aminobenzonitrile to prepare quinazoline-2,4(1*H*,3*H*)-diones were investigated under optimal reaction conditions reported in our previous work.<sup>22</sup> For example, 2-aminobenzonitrile ( $4\text{ mmol}$ ) and  $[P_{4442}]_2[Hy]$  ( $0.8\text{ mmol}$ ) were added to a round bottom flask containing a magnet.  $CO_2$  was passed through to remove the air in the flask. A  $CO_2$  balloon was connected to the flask, and the  $CO_2$  pressure was ensured to be  $0.1\text{ MPa}$  and the mixture was stirred at  $353.15\text{ K}$ . The progress of the reaction was monitored by HPLC (Zorbax RX-C8 column, the mobile phase was acetonitrile: water = 5 : 5 in volume ratio and the detection wavelength  $\lambda$  was  $245\text{ nm}$ ) and the content of quinazoline-2,4(1*H*,3*H*)-diones was determined using the external standard method to calculate the product yield.

#### Computation method

The DFT calculations were performed using the Gaussian 09 D.01 program,<sup>26</sup> with geometry optimizations and interaction energy calculations at the B3LYP-D3/6-31++G (d, p) basis set level.<sup>27</sup> The optimized geometry of  $[P_{4442}][Hy]$  and  $[P_{4442}][Hy-CO_2]$  ion pairs,  $[Hy]^-$ ,  $[Hy]^{2-}$ ,  $CO_2$ ,  $[Hy-CO_2]^-$ ,  $[Hy-2CO_2]^{2-}$ , chain-like intermolecular hydrogen bonding of  $[Hy]^-$ , and six-membered cyclic quasi-intramolecular hydrogen bond formed by  $[Hy-CO_2]^-$  was considered to be a local minimum with no imaginary frequencies. The energies of chain-like intermolecular hydrogen bonding of  $[Hy]^-$  and  $[P_{4442}][Hy]$  and  $[P_{4442}][Hy-CO_2]$  ion pairs, the interactions between  $[Hy]^-$  and  $CO_2$ , six-membered cyclic quasi-intramolecular hydrogen bond formed by  $[Hy-CO_2]^-$ , and the interactions between  $[Hy]^{2-}$  and  $CO_2$ , were calculated with the basis set superposition error (BSSE) corrections,<sup>28,29</sup> where the enthalpy ( $\Delta H$ ) and Gibbs free energy ( $\Delta G$ ) were calculated as the difference between the energy of the complex and the sum of the energies of the optimized monomers. Using the approaches described by Katsyuba and co-workers,<sup>30</sup> the energies of chain-like intermolecular hydrogen bonding of  $[Hy]^-$  were extracted and the method is described in the ESI†. The Cartesian coordinates of the optimized structures are shown in Fig. S1 (ESI†).

## 3. Results and discussion

#### Comparison of physical properties of hydantoin-based ILs

$^1H$  NMR data of  $[P_{4442}][Br]$  and hydantoin-based ILs are found to be in good agreement with their corresponding chemical structures (Fig. S2, ESI†). The TGA curves of the three hydantoin-based ILs show that they have good thermal stability, and the decomposition temperature is higher than  $200\text{ }^\circ\text{C}$  (Fig. S3, ESI†). Among them,  $[P_{4442}][Hy]$  has the best thermal stability, while  $[HDBU][Hy]$  has relatively weak thermal stability.

At room temperature ( $\sim 298\text{ K}$ ),  $[P_{4442}]_2[Hy]$  is a liquid,  $[HDBU][Hy]$  is a gel, while  $[P_{4442}][Hy]$  is a solid (Fig. S4, ESI†). As shown in Fig. S5 (ESI†), the melting points of  $[P_{4442}][Hy]$  and

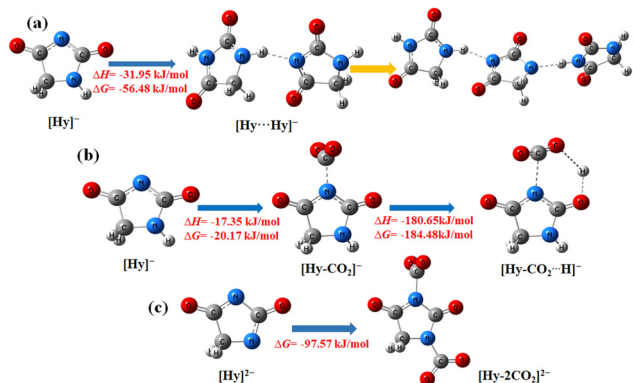


Fig. 1 The optimized geometry and the calculated energy. (a) Chain-like intermolecular hydrogen bonding of  $[\text{Hy}]^-$ ; (b)  $\text{CO}_2$  absorption by  $[\text{Hy}]^-$  and quasi-intramolecular cyclic hydrogen bonds formed by  $[\text{Hy-CO}_2]^-$  and the active hydrogen atom; (c) double-site interaction between  $[\text{Hy}]^-$  and  $\text{CO}_2$ .

$[\text{HDBU}][\text{Hy}]$  are 325.20 and 358.39 K (onset temperature), respectively. As shown in Fig. S6 (ESI<sup>†</sup>),  $\eta$  of  $[\text{P}_{4442}][\text{Hy}]$  is larger than that of  $[\text{P}_{4442}]_2[\text{Hy}]$ . The differences in melting point and  $\eta$  of three hydantoin-based ILs may be attributed to the role of the active hydrogen atom in  $[\text{Hy}]^-$ . To reveal the effect of the active hydrogen atom, the structure of  $[\text{Hy}]^-$  is optimized using DFT calculations (Fig. 1a), which shows that the active hydrogen atom in  $[\text{Hy}]^-$  can spontaneously form chain-like intermolecular hydrogen bonds with the  $\text{N}^-$  atom of another anion with  $\Delta G = -56.48 \text{ kJ mol}^{-1}$ , leading to an increase in the melting point and  $\eta$ .<sup>1</sup> In addition, the active hydrogen atom in  $[\text{Hy}]^-$  of  $[\text{P}_{4442}][\text{Hy}]$  tends to form hydrogen-bonded aggregates of multiple anions, which is different from the formation of bimolecular hydrogen bonding between the active hydrogen in the cation and the anion of PILs.<sup>5–7</sup> This is the main reason why  $[\text{P}_{4442}][\text{Hy}]$  with an active hydrogen atom in the anion is a solid, whereas most PILs with the active hydrogen atom in the cation are liquids at room temperature. When the active hydrogen atom in  $[\text{Hy}]^-$  of  $[\text{P}_{4442}][\text{Hy}]$  is replaced by a methyl group, the obtained  $[\text{P}_{4442}][1\text{-MHy}]$  is a liquid with  $\eta$  of 182.74 cp at 318.15 K,<sup>21</sup> confirming that the active hydrogen atom in  $[\text{Hy}]^-$  leads to an increase in the melting point and  $\eta$  of  $[\text{P}_{4442}][\text{Hy}]$  through the formation of chain-like intermolecular hydrogen bonding. Due to the presence of active hydrogen in both anions and cations,  $[\text{HDBU}][\text{Hy}]$  has a higher melting point than  $[\text{P}_{4442}][\text{Hy}]$ .

As shown in Fig. 2, the degree of red-shift of the wavenumber of N–H in the IL + pyrrole mixture indicates that the basicity of hydantoin-based ILs is as follows:  $[\text{P}_{4442}]_2[\text{Hy}] > [\text{P}_{4442}][\text{Hy}] > [\text{HDBU}][\text{Hy}]$ , suggesting that the active hydrogen atom in the anion plays an important role in the basicity. The basicity of  $[\text{P}_{4442}][\text{Hy}]$  is weaker than that of  $[\text{P}_{4442}]_2[\text{Hy}]$ , due to hydrogen bond interactions of the active hydrogen atom in  $[\text{Hy}]^-$  with the basicity center  $\text{N}^-$  atom of  $[\text{Hy}]^-$ . Because the active hydrogen atoms in both the cation and anion can form hydrogen bond interactions with the  $\text{N}^-$  atom of  $[\text{Hy}]^-$ , the basicity of  $[\text{HDBU}][\text{Hy}]$  is the weakest. By comparing the  $\text{CO}_2$  capture capacity of  $[\text{HMTBD}][\text{Im}]$  and  $[\text{P}_{66614}][\text{Im}]$ , it is known that the

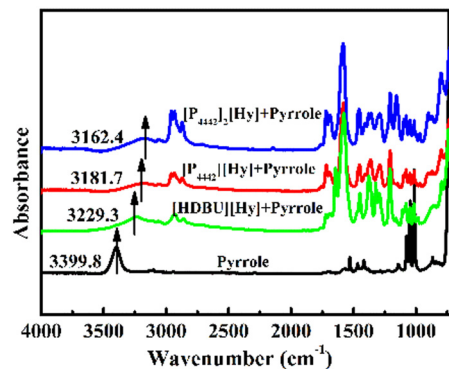


Fig. 2 FT-IR spectra of pure pyrrole and the IL + pyrrole mixture.

active hydrogen atom in the cation has a weak effect on the basicity,<sup>5,6</sup> whereas the present results show that the active hydrogen atom in the anion can weaken the basicity of ILs, which seems to indicate that the basicity of ILs can be modulated by the position of the active hydrogen atom.

### $\text{CO}_2$ absorption behaviour and the absorption mechanism of $[\text{P}_{4442}][\text{Hy}]$ and $[\text{P}_{4442}]_2[\text{Hy}]$

As shown in Fig. 3, the  $\text{CO}_2$  absorption capacity of  $[\text{P}_{4442}][\text{Hy}]$  and  $[\text{P}_{4442}]_2[\text{Hy}]$  decreases with increasing temperature, and the saturation capacity at 303 K is 0.84 and 1.90 mol  $\text{CO}_2$  per mol IL, respectively. Interestingly, when  $\text{CO}_2$  is poured into  $[\text{P}_{4442}][\text{Hy}]$  at 303 K and stirred,  $[\text{P}_{4442}][\text{Hy}]$  changes from a solid to a liquid with a gradual decrease in  $\eta$  (Fig. S4, ESI<sup>†</sup>), which is different from the increase in  $\eta$  of PILs with  $\text{CO}_2$  absorption,<sup>7</sup> while  $[\text{HDBU}][\text{Hy}]$  remains a gel in the same situation. The  $\eta$  of  $[\text{P}_{4442}][\text{Hy-CO}_2]$  at saturation is 506.4 cp at 315.15 K, which is lower than the  $\eta$  of the pure  $[\text{P}_{4442}][\text{Hy}]$ . The interaction energies of  $[\text{P}_{4442}][\text{Hy}]$  and  $[\text{P}_{4442}][\text{Hy-CO}_2]$  ion pairs (Fig. S7, ESI<sup>†</sup>) show a decrease in the interaction between the anion and cation after  $\text{CO}_2$  absorption by  $[\text{P}_{4442}][\text{Hy}]$ , which may be a reason for the decrease in  $\eta$  of  $[\text{P}_{4442}][\text{Hy-CO}_2]$ . Unlike  $[\text{P}_{4442}]_2[\text{Hy}]$ , the  $\text{CO}_2$  capture capacity of  $[\text{P}_{4442}][\text{Hy}]$  does not reach equimolar absorption. It is clear that the  $\text{CO}_2$  absorption behaviour of  $[\text{P}_{4442}][\text{Hy}]$  is different from that of  $[\text{P}_{4442}]_2[\text{Hy}]$  and  $[\text{HDBU}][\text{Hy}]$ , so it is worth investigating the  $\text{CO}_2$  absorption mechanism of  $[\text{P}_{4442}][\text{Hy}]$ .

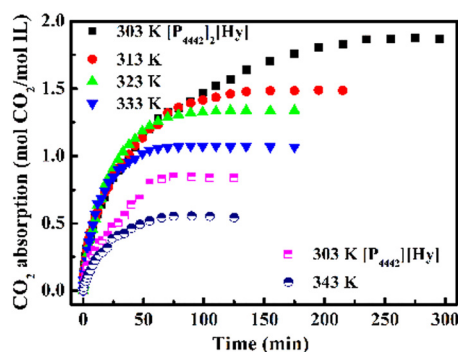
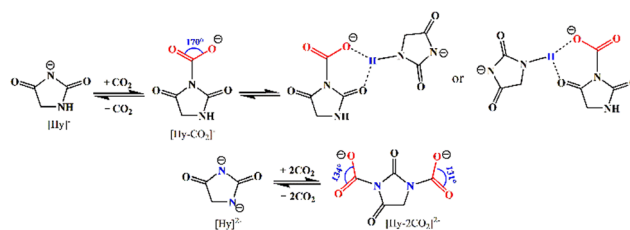


Fig. 3  $\text{CO}_2$  absorption behavior of  $[\text{P}_{4442}][\text{Hy}]$  and  $[\text{P}_{4442}]_2[\text{Hy}]$  at 0.1 MPa.

As shown in Fig. 4, a new peak at  $1714\text{ cm}^{-1}$  appears in FT-IR spectra of  $[\text{P}_{4442}][\text{Hy-CO}_2]$ , accompanied by a new resonance peak at  $162.6\text{ ppm}$  in the  $^{13}\text{C}$  NMR spectrum, indicating the formation of a new carbonyl by chemical interaction of the  $\text{N}^-$  atom in  $[\text{Hy}]^-$  with  $\text{CO}_2$ .<sup>21</sup> Furthermore, the broad peak at  $3220\text{ cm}^{-1}$  of  $[\text{P}_{4442}][\text{Hy}]$  in the FT-IR spectra, which is attributed to the stretching vibration peak of N-H of the intermolecular hydrogen bond of  $[\text{Hy}]^-$ , gradually disappears after  $\text{CO}_2$  absorption, together with the weakening of the intensity of the original  $\text{C=O}$  of  $[\text{Hy}]^-$  at  $1585\text{ cm}^{-1}$ , suggesting that N-H and  $\text{C=O}$  may have interacted simultaneously with the  $\text{CO}_2$  absorbed by the anion. Correspondingly, the original  $\text{C=O}$  of  $[\text{Hy}]^-$  in the  $^{13}\text{C}$  NMR spectra at  $191.2$  and  $175.0\text{ ppm}$  shifts to a lower field and appears at  $179.0$  and  $160.1\text{ ppm}$  after  $\text{CO}_2$  absorption. Therefore, considering the formation of a new  $\text{C=O}$  and the changes in the original N-H and  $\text{C=O}$  in  $[\text{Hy}]^-$  after  $\text{CO}_2$  absorption, as well as the decrease in  $\eta$  of  $[\text{P}_{4442}][\text{Hy}]$  after  $\text{CO}_2$  absorption, the following  $\text{CO}_2$  absorption mechanism is proposed (Scheme 2): The  $\text{N}^-$  atom of  $[\text{Hy}]^-$  first interacts with  $\text{CO}_2$  to form carbamate carbonyl, and then a six-membered cyclic hydrogen bond is formed between the original  $\text{C=O}$  in  $[\text{Hy}]^-$  and the  $\text{O}^-$  atom in the carbamate carbonyl as well as the active hydrogen atom. To further confirm the mechanism, the formed intermediates and hydrogen bonds are optimized using DFT calculations. As shown in Fig. 1b,  $\Delta H$  and  $\Delta G$  for the interaction of the  $\text{N}^-$  atom in  $[\text{Hy}]^-$  with  $\text{CO}_2$  are  $-17.35$  and  $-20.17\text{ kJ mol}^{-1}$ , respectively. Interestingly, the  $[\text{Hy-CO}_2]^-$  intermediate can spontaneously form stable cyclic quasi-intramolecular bonds with  $\Delta H$  and  $\Delta G$  of  $-180.65$  and  $-184.48\text{ kJ mol}^{-1}$ , respectively. Therefore, the combination of  $\text{CO}_2$  absorption experiments, spectroscopy and DFT calculations suggests that the sub-equimolar  $\text{CO}_2$  capture capacity of  $[\text{P}_{4442}][\text{Hy}]$  is due to the  $\text{N}^-$  atom of  $[\text{Hy}]^-$  being partially occupied by the active hydrogen atom through the occurrence of chain-like hydrogen bond interactions (Fig. 1a). When  $\text{CO}_2$  is absorbed, the original chain-like intermolecular hydrogen bonds are converted into cyclic quasi-intramolecular hydrogen bonds, resulting in a decrease in  $\eta$ .<sup>31–33</sup> As the original N-H and  $\text{C=O}$  groups of  $[\text{Hy}]^-$  are involved in the formation of the cyclic hydrogen bonds of  $[\text{Hy-CO}_2]^-$ , their infrared absorption intensity is weakened and the chemical shift is shifted to higher fields.

In addition, the  $\text{CO}_2$  absorbed by  $[\text{P}_{4442}][\text{Hy}]$  can be easily desorbed by heating, and then  $[\text{P}_{4442}][\text{Hy}]$  is regenerated and



Scheme 2 Possible mechanism of  $\text{CO}_2$  absorption by  $[\text{P}_{4442}][\text{Hy}]$  and  $[\text{P}_{4442}]_2[\text{Hy}]$ .

returned to the solid state. As shown in Fig. 5a, five cycles of absorption/desorption indicate that  $[\text{P}_{4442}][\text{Hy}]$  has good reusability. Therefore, considering the good reusability and the change of state during  $\text{CO}_2$  absorption-desorption,  $[\text{P}_{4442}][\text{Hy}]$  is a potential  $\text{CO}_2$ -responsive molecular switch,<sup>34,35</sup> resulting from the contribution of the active hydrogen atom in  $[\text{Hy}]^-$ .

Although  $[\text{P}_{4442}][\text{Hy}]$  has the potential to be a  $\text{CO}_2$ -response molecular switch, the hydrogen-bonded aggregates formed by the active hydrogen atoms are unfavorable for  $\text{CO}_2$  capture. When the active hydrogen atom in  $[\text{Hy}]^-$  is neutralized to dual anion  $[\text{Hy}]^{2-}$ ,  $[\text{P}_{4442}]_2[\text{Hy}]$  is not only less viscous (Fig. S6, ESI<sup>†</sup>), but also exhibits an excellent  $\text{CO}_2$  absorption capacity (Fig. 3), which is larger than those of other dual anion ILs such as  $[\text{P}_{4442}]_2[\text{L-Ser}]$  (1.10 mol  $\text{CO}_2$  per mol IL at  $298\text{ K}$ ) and  $[\text{P}_{4442}]_2[\text{IDA}]$  (1.69 mol  $\text{CO}_2$  per mol IL at  $313\text{ K}$ ).<sup>31,36</sup> Therefore, the  $\text{CO}_2$  absorption mechanism of  $[\text{P}_{4442}]_2[\text{Hy}]$  is investigated. As shown in Fig. 6, the FT-IR spectra of  $\text{CO}_2$ -absorbed  $[\text{P}_{4442}]_2[\text{Hy}]$  show two new peaks at  $1716$  and  $1616\text{ cm}^{-1}$ , and its  $^{13}\text{C}$  NMR spectrum also shows two new peaks at  $158.9$  and  $153.7\text{ ppm}$ , indicating that the two  $\text{N}^-$  atoms in  $[\text{Hy}]^{2-}$  can chemically interact with  $\text{CO}_2$ , thus realizing the efficient absorption of  $\text{CO}_2$  through the double-site interaction. The TGA curve of  $[\text{P}_{4442}]_2[\text{Hy-CO}_2]$

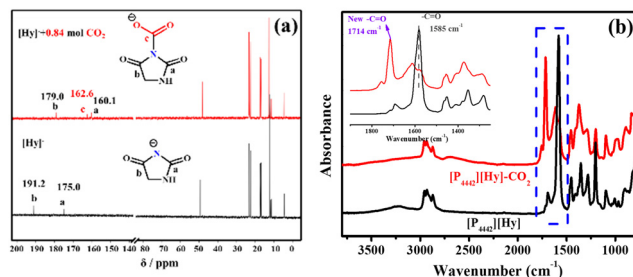


Fig. 4  $^{13}\text{C}$  NMR (a) and FT-IR (b) spectra of  $[\text{P}_{4442}][\text{Hy}]$  before and after  $\text{CO}_2$  capture.

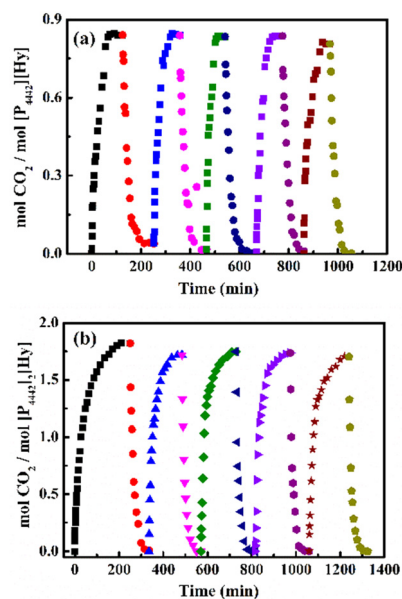


Fig. 5  $\text{CO}_2$  absorption/desorption by  $[\text{P}_{4442}][\text{Hy}]$  (a) and  $[\text{P}_{4442}]_2[\text{Hy}]$  (b) at  $303\text{ K}$  and release at  $343\text{ K}$  under  $\text{N}_2$ .

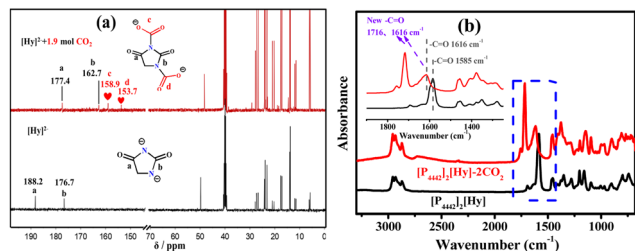


Fig. 6  $^{13}\text{C}$  NMR (a) and FT-IR (b) of  $[\text{P}_{4442}]_2[\text{Hy}]$  before and after  $\text{CO}_2$  capture.

shows two weight loss peaks (Fig. S3b, ESI $^\dagger$ ), confirming that  $[\text{P}_{4442}]_2[\text{Hy}]$  can absorb  $\text{CO}_2$  through the double-site interaction. Accordingly, the  $\text{CO}_2$  absorption mechanism of  $[\text{P}_{4442}]_2[\text{Hy}]$  is proposed (Scheme 2), and the structure of  $[\text{Hy}-2\text{CO}_2]^{2-}$  is optimized by DFT calculations with  $\Delta G$  of  $-97.57 \text{ kJ mol}^{-1}$  (Fig. 1c).

The effects of  $\text{CO}_2$  partial pressure and temperature on the  $\text{CO}_2$  absorption by  $[\text{P}_{4442}]_2[\text{Hy}]$  are investigated and are shown in Fig. S8a (ESI $^\dagger$ ). As the  $\text{CO}_2$  partial pressure decreases from 0.1 to 0.02 MPa, the saturation absorption capacity of  $[\text{P}_{4442}]_2[\text{Hy}]$  at 303 K decreases from 1.90 to 1.55 mol  $\text{CO}_2$  per mol IL, but it still shows a good absorption capacity, indicating that  $[\text{P}_{4442}]_2[\text{Hy}]$  has the potential to absorb low concentrations of  $\text{CO}_2$ . The saturation absorption capacity of  $[\text{P}_{4442}]_2[\text{Hy}]$  at different partial pressures and temperatures is plotted in Fig. S8b (ESI $^\dagger$ ), showing that the effect of temperature is greater than that of partial pressure. Based on the saturated absorption capacity at 303–333 K and 0.02 MPa, combined with the van der Hoff equation (Fig. S8c, ESI $^\dagger$ ), the absorption enthalpy of  $\text{CO}_2$  of  $[\text{P}_{4442}]_2[\text{Hy}]$  is obtained to be  $-58.62 \text{ kJ mol}^{-1}$ , which is lower than that of  $[\text{P}_{66614}]_2[\text{Asp}]$  ( $-223 \text{ kJ mol}^{-1}$ ) and  $[\text{P}_{4442}]_2[\text{IDA}]$  ( $-141.8 \text{ kJ mol}^{-1}$ ).<sup>36,37</sup> Due to the lower absorption enthalpy,  $[\text{P}_{4442}]_2[\text{Hy}]$  shows good absorption-desorption ability (Fig. 5b). Furthermore, the FT-IR spectra of pure and received  $[\text{P}_{4442}]_2[\text{Hy}]$  compared in Fig. S9 (ESI $^\dagger$ ) show that  $[\text{P}_{4442}]_2[\text{Hy}]$  has excellent reusability, suggesting that  $[\text{P}_{4442}]_2[\text{Hy}]$  has the ability to activate and catalyze  $\text{CO}_2$  conversion.<sup>38–40</sup>

### Comparison of the catalytic $\text{CO}_2$ conversion performance of hydantoin-based ILs

According to the literature,<sup>41–43</sup> when  $\text{CO}_2$  is activated by the catalyst, the O–C–O angle decreases from  $180^\circ$  to about  $130^\circ$ , and the weaker the activation is when the O–C–O angle tends to be  $180^\circ$ . The optimized structures of the intermediates by DFT calculations show that the O–C–O angle of  $[\text{Hy}-2\text{CO}_2]^{2-}$  is close to  $130^\circ$  (Scheme 2), while that of  $[\text{Hy}-\text{CO}_2]^-$  is  $170^\circ$  (Scheme 2), resulting from the formation of the six-membered ring hydrogen bond. The difference in the O–C–O angle in  $[\text{Hy}-\text{CO}_2]^-$  and  $[\text{Hy}-2\text{CO}_2]^{2-}$  seems to indicate that the active hydrogen atom of  $[\text{Hy}]^-$  is unfavorable for  $\text{CO}_2$  activation and subsequent conversion.

To confirm the above speculation, the reactions of  $\text{CO}_2$  with 2-aminobenzonitrile catalyzed by  $[\text{P}_{4442}][\text{Hy}]$ ,  $[\text{P}_{4442}]_2[\text{Hy}]$ , and  $[\text{HDBU}][\text{Hy}]$  under solvent-free conditions at 0.1 MPa  $\text{CO}_2$  are studied (Fig. S10, ESI $^\dagger$ ). The optimal reaction conditions are listed in Table 1 and compared with the reported data, and the

Table 1 The reaction of  $\text{CO}_2$  with 2-aminobenzonitrile catalysed by ILs at 0.1 MPa  $\text{CO}_2$ <sup>a</sup>

Entry	ILs	Time (h)	yield (%)	Ref.
1	$[\text{P}_{4442}]_2[\text{Hy}]$	24	98	This work
2	$[\text{P}_{4442}][\text{Hy}]$	24	84	This work
3	$[\text{P}_{4442}][\text{Hy}]$	46	94	This work
4	$[\text{HDBU}][\text{Hy}]$	24	72	This work
5	$[\text{HDBU}][\text{Hy}]$	43	73	This work
6	$[\text{P}_{4442}][1\text{-MHy}]$	24	92	21
7	$[\text{P}_{4442}][1\text{-MHy}]$	30	97	21
8	$[\text{HTMG}][\text{Suc}]$	10	89.2 <sup>b</sup>	16
9	$[\text{BzTMA}][\text{Suc}]$	10	98.8 <sup>b</sup>	16
10	$[\text{Ch}][\text{Im}]$	20	98 <sup>c</sup>	38

<sup>a</sup> Reaction conditions: 20 mol% of IL to 2-aminobenzonitrile, 353.15 K, without solvent, HPLC yield. <sup>b</sup> 100 mol% of IL to 2-aminobenzonitrile, 343.15 K, with DMSO. <sup>c</sup> 100 mol% of IL to 2-aminobenzonitrile.

sequence of the catalytic properties of ILs over 24 h is as follows:  $[\text{P}_{4442}]_2[\text{Hy}] > [\text{P}_{4442}][\text{Hy}] > [\text{HDBU}][\text{Hy}]$ , indicating that the active hydrogen atom in  $[\text{Hy}]^-$  may weaken the catalytic properties. From our previous work,<sup>22</sup> it is known that the  $[\text{Hy}]^{2-}$  of  $[\text{P}_{4442}]_2[\text{Hy}]$  simultaneously activates  $\text{CO}_2$  and  $-\text{NH}_2$  of 2-aminobenzonitrile through its basic center  $\text{N}^-$  atom to realize the efficient catalytic properties. In the case of  $[\text{P}_{4442}][\text{Hy}]$ , the anion basic center  $\text{N}^-$  atom of  $[\text{Hy}]^-$  is easily occupied by other active hydrogen atoms through intermolecular hydrogen bonding, which will reduce its ability to activate both  $\text{CO}_2$  and  $-\text{NH}_2$  and lead to the decrease of the catalytic performance. In addition, the absorbed  $\text{CO}_2$  in  $[\text{Hy}-\text{CO}_2]^-$  forms cyclic quasi-intramolecular hydrogen bonds with the active hydrogen atom, which reduces  $\eta$  but does not favor  $\text{CO}_2$  activation. Replacing the active hydrogen atom in  $[\text{Hy}]^-$  with a methyl group improves the catalytic performance of  $[\text{P}_{4442}][1\text{-MHy}]$ ,<sup>21</sup> confirming that the active hydrogen atom is detrimental to the catalytic performance of  $[\text{P}_{4442}][\text{Hy}]$ . Moreover, comparison of entries 1–2 reveals that the presence of the active hydrogen atom in the anion reduces the product yield by 14%, while entries 8–9 show that the presence of the active hydrogen atom in the cation reduces the yield by 9.6%, indicating that the effects of the active hydrogen atom in the anion on the catalytic ability of ILs are slightly greater than those of the active hydrogen atom in the cation. Therefore, it is not difficult to understand why  $[\text{HDBU}][\text{Hy}]$  shows the worst catalytic performance given the presence of both active hydrogen atoms on its anion and cation. As can be seen from entries 1 and 10, the amount of  $[\text{P}_{4442}]_2[\text{Hy}]$  is much smaller than that of  $[\text{Ch}][\text{Im}]$  at similar yields,<sup>38</sup> i.e., the catalytic properties of the former are better than those of the latter, due to the fact that the absorbed  $\text{CO}_2$  is more easily desorbed in the former than in the latter,<sup>38</sup> and also indicating that the ability to activate  $\text{CO}_2$  is better for  $[\text{P}_{4442}]_2[\text{Hy}]$  than for  $[\text{Ch}][\text{Im}]$ . Therefore, when designing ILs for  $\text{CO}_2$  uptake and chemical conversion, it is necessary to consider not only the effect of the active hydrogen atom in the cation, but also the effect of the active hydrogen atom in the anion.

## Conclusions

The present study shows that the active hydrogen atom in  $[\text{Hy}]^-$  of  $[\text{P}_{4442}][\text{Hy}]$  can form chain-like intermolecular hydrogen bonds with the  $\text{N}^-$  atom, which causes the basicity center of  $[\text{Hy}]^-$  to be occupied, leading to an increase in the melting point, a decrease in the basicity, and ultimately a decrease in  $\text{CO}_2$  capture capacity and catalytic  $\text{CO}_2$  conversion performance. Interestingly,  $[\text{P}_{4442}][\text{Hy}]$  exhibits a solid/liquid two-phase transition during  $\text{CO}_2$  absorption/desorption due to the formation of quasi-intramolecular hydrogen bonding between the active hydrogen atom and the  $\text{O}^-$  atom of the absorbed  $\text{CO}_2$ , suggesting that the presence of the active hydrogen atom gives  $[\text{P}_{4442}][\text{Hy}]$  the potential to be an excellent molecular switch. Since there is no active hydrogen atom in the anion of  $[\text{P}_{4442}]_2[\text{Hy}]$ , it shows excellent carbon capture and conversion performance through the double-site interaction. The results suggest that the active hydrogen atom in the anion plays an important role in the properties and potential applications of ILs, which is different from the role of the active hydrogen atom in the cation.

## Author contributions

Tingting Chen: conceptualization, investigation, and writing (original draft). Zhongyuan Sun: investigation and visualization. Yujun Guo: data curation, validation, and formal analysis. Yingjie Xu: supervision, writing (review & editing), funding acquisition, and resources.

## Conflicts of interest

There are no conflicts to declare.

## Acknowledgements

This work was supported by the National Natural Science Foundation of China (No. 21978172).

## References

- 1 T. L. Greaves and C. J. Drummond, Protic ionic liquids: properties and applications, *Chem. Rev.*, 2008, **108**, 206–237.
- 2 D. H. Zaitsau, V. N. Emel'yanenko, P. Stange, C. Schick, S. P. Verevkin and R. Ludwig, Dispersion and hydrogen bonding rule: why the vaporization enthalpies of aprotic ionic liquids are significantly larger than those of protic ionic liquids, *Angew. Chem., Int. Ed.*, 2016, **55**, 11682–11686.
- 3 M. Yoshizawa, W. Xu and C. A. Angell, Ionic liquids by proton transfer: vapor pressure, conductivity, and the relevance of  $\Delta pK_a$  from aqueous solutions, *J. Am. Chem. Soc.*, 2003, **125**, 15411–15419.
- 4 D. R. MacFarlane, J. M. Pringle, K. M. Johansson, S. A. Forsyth and M. Forsyth, Lewis base ionic liquids, *Chem. Commun.*, 2006, 1905–1917.
- 5 C. Wang, H. Luo, D.-E. Jiang, H. Li and S. Dai, Carbon dioxide capture by superbase-derived protic ionic liquids, *Angew. Chem., Int. Ed.*, 2010, **49**, 5978–5981.
- 6 C. Wang, X. Luo, H. Luo, D.-E. Jiang, H. Li and S. Dai, Tuning the basicity of ionic liquids for equimolar  $\text{CO}_2$  capture, *Angew. Chem., Int. Ed.*, 2011, **50**, 4918–4922.
- 7 Y. Xu,  $\text{CO}_2$  absorption behavior of azole-based protic ionic liquids: influence of the alkalinity and physicochemical properties, *J. CO<sub>2</sub> Util.*, 2017, **19**, 1–8.
- 8 X. Lei, Y. Xu, L. Zhu and X. Wang, Highly efficient and reversible  $\text{CO}_2$  capture through 1, 1, 3, 3-tetramethylguanidinium imidazole ionic liquid, *RSC Adv.*, 2014, **4**, 7052–7057.
- 9 G. Cui, J. Wang and S. Zhang, Active chemisorption sites in functionalized ionic liquids for carbon capture, *Chem. Soc. Rev.*, 2016, **45**, 4307–4339.
- 10 P. A. Hunt, C. R. Ashworth and R. P. Matthews, Hydrogen bonding in ionic liquids, *Chem. Soc. Rev.*, 2015, **44**, 1257–1288.
- 11 J. Ma, Y. Wang, X. Yang, M. Zhu and B. Wang, DFT study on the chemical absorption mechanism of  $\text{CO}_2$  in diamino protic ionic liquids, *J. Phys. Chem. B*, 2021, **125**, 1416–1428.
- 12 K. E. Gutowski and E. J. Maginn, Amine-functionalized task-specific ionic liquids: a mechanistic explanation for the dramatic increase in viscosity upon complexation with  $\text{CO}_2$  from molecular simulation, *J. Am. Chem. Soc.*, 2008, **130**, 14690–14704.
- 13 E. I. Izgorodina, J. L. Hodgson, D. C. Weis, S. J. Pas and D. R. MacFarlane, Physical absorption of  $\text{CO}_2$  in protic and aprotic ionic liquids: an interaction perspective, *J. Phys. Chem. B*, 2015, **119**, 11748–11759.
- 14 Y. Zhao, B. Yu, Z. Yang, H. Zhang, L. Hao, X. Gao and Z. Liu, A protic ionic liquid catalyzes  $\text{CO}_2$  conversion at atmospheric pressure and room temperature: synthesis of quinazoline-2, 4(1H, 3H)-diones, *Angew. Chem., Int. Ed.*, 2014, **53**, 5922–5925.
- 15 X. Mu, L. Han and T. Liu, How and why a protic ionic liquid efficiently catalyzes chemical fixation of  $\text{CO}_2$  to quinazoline-2, 4(1H, 3H)-diones: electrostatically controlled reactivity, *J. Phys. Chem. A*, 2019, **123**, 9394–9402.
- 16 T. Wang, D. Zheng, Z. Zhang, L. Wang and J. Zhang, Exploration of catalytic species for highly efficient preparation of quinazoline-2, 4(1H, 3H)-diones by succinimide-based ionic liquids under atmospheric pressure: combination of experimental and theoretical study, *Fuel*, 2022, **319**, 123628.
- 17 J. Qiu, Y. Zhao, Z. Li, H. Wang, M. Fan and J. Wang, Efficient ionic-liquid-promoted chemical fixation of  $\text{CO}_2$  into  $\alpha$ -alkylidene cyclic carbonates, *ChemSusChem*, 2017, **10**, 1120–1127.
- 18 W. Sun, M. Wang, Y. Zhang, W. Ding, F. Huo, L. Wei and H. He, Protic vs aprotic ionic liquid for  $\text{CO}_2$  fixation: a simulation study, *Green Energy Environ.*, 2020, **5**, 183–194.
- 19 K. Dong, S. Zhang and J. Wang, Understanding the hydrogen bonds in ionic liquids and their roles in properties and reactions, *Chem. Commun.*, 2016, **52**, 6744–6764.
- 20 J. Hu, J. Ma, Q. Zhu, Z. Zhang, C. Wu and B. Han, Transformation of atmospheric  $\text{CO}_2$  Catalyzed by protic ionic

- liquids: efficient synthesis of 2-oxazolidinones, *Angew. Chem., Int. Ed.*, 2015, **54**, 5399–5403.
- 21 T. Chen, Y. Zhang and Y. Xu, Efficient synthesis of quinazoline-2, 4(1*H*, 3*H*)-dione *via* simultaneous activated CO<sub>2</sub> and 2-aminobenzonitrile by 1-methylhydantoin anion-functionalized ionic liquid through the multiple-site cooperative interactions, *ACS Sustainable Chem. Eng.*, 2022, **10**, 10699–10711.
  - 22 T. Chen, Y. Guo and Y. Xu, Efficient catalytic conversion of CO<sub>2</sub> and 2-aminobenzonitrile to quinazoline-2,4(1*H*,3*H*)-diones by dual-site anion-functionalized ionic liquids: a reconsideration of the mechanisms, *Chem. Commun.*, 2023, **59**, 12282–12285.
  - 23 H. Shu and Y. Xu, Tuning the strength of cation coordination interactions of dual functional ionic liquids for improving CO<sub>2</sub> capture performance, *Int. J. Greenhouse Gas Control*, 2020, **94**, 102934.
  - 24 J. Liu, X. Tang, H. Lu and Y. Xu, Insight into the interactions between azole-anion-based ionic liquids and propargylic alcohol: influence on the carboxylative cyclization of propargylic alcohol with carbon dioxide, *ACS Sustainable Chem. Eng.*, 2021, **9**, 5050–5060.
  - 25 C. Binet, A. Jadi, J. Lamotte and J. C. Lavalley, Use of pyrrole as an IR spectroscopic molecular probe in a surface basicity study of metal oxides, *J. Chem. Soc., Faraday Trans.*, 1996, **92**, 123–129.
  - 26 M. Frisch, G. Trucks, H. Schlegel, G. Scuseria, M. Robb, J. Cheeseman, G. Scalmani, V. Barone, B. Mennucci and G. A. Petersson, *et al.*, *Gaussian 09, Revision D.01*, Gaussian Inc., Wallingford, CT, 2009.
  - 27 S. Grimme, J. Antony, S. Ehrlich and H. Krieg, A consistent and accurate *ab initio* parametrization of density functional dispersion correction (DFT-D) for the 94 elements H-Pu, *J. Chem. Phys.*, 2010, **132**, 154104.
  - 28 C. Deligkaris and J. H. Rodriguez, Correction to DFT interaction energies by an empirical dispersion term valid for a range of intermolecular distances, *Phys. Chem. Chem. Phys.*, 2012, **14**, 3414–3424.
  - 29 D. Si, K. Chen, J. Yao and H. Li, Structures and electronic properties of lithium chelate-based ionic liquids, *J. Phys. Chem. B*, 2016, **120**, 3904–3913.
  - 30 S. A. Katsyuba, M. V. Vener, E. E. Zvereva, Z. Fei, R. Scopelliti, J. G. Brandenburg, S. Siankevich and P. J. Dyson, Quantification of conventional and nonconventional charge-assisted hydrogen bonds in the condensed and gas phases, *J. Phys. Chem. Lett.*, 2015, **6**, 4431–4436.
  - 31 M. Pan, Y. Zhao, X. Zeng and J. Zou, Efficient absorption of CO<sub>2</sub> by introduction of intramolecular hydrogen bonding in chiral amino acid ionic liquids, *Energy Fuels*, 2018, **32**, 6130–6135.
  - 32 W.-J. Jiang, F.-Y. Zhong, L.-S. Zhou, H.-L. Peng, J.-P. Fan and K. Huang, Chemical dual-site capture of NH<sub>3</sub> by unprecedentedly low-viscosity deep eutectic solvents, *Chem. Commun.*, 2020, **56**, 2399–2402.
  - 33 S. Sarkar, A. Shil, Y. W. Jun, Y. J. Yang, W. Choi, S. Singha and K. H. Ahn, Interactive twin intramolecular hydrogen bonds enable bright, S-Blue emissive, environment-insensitive single-benzene fluorophores, *Adv. Funct. Mater.*, 2023, **33**, 2304507.
  - 34 X. Pei, Z. Li, H. Wang, Q. Zhou, Z. Liu and J. Wang, CO<sub>2</sub>-switchable phase separation of nonaqueous surfactant-free ionic liquid-based microemulsions, *ACS Sustainable Chem. Eng.*, 2022, **10**, 1777–1785.
  - 35 S. Dowlati, R. Mokhtari, L. Hohl, R. Miller and M. Kraume, Advances in CO<sub>2</sub>-switchable surfactants towards the fabrication and application of responsive colloids, *Adv. Colloid Interface Sci.*, 2023, 102907.
  - 36 F. F. Chen, K. Huang, Y. Zhou, Z. Q. Tian, X. Zhu, D. J. Tao, D. E. Jiang and S. Dai, Multi-molar absorption of CO<sub>2</sub> by the activation of carboxylate groups in amino acid ionic liquids, *Angew. Chem., Int. Ed.*, 2016, **55**, 7166–7170.
  - 37 X. Luo, X. Lv, G. Shi, Q. Meng, H. Li and C. Wang, Designing amino-based ionic liquids for improved carbon capture: one amine binds two CO<sub>2</sub>, *AIChE J.*, 2019, **65**, 230–238.
  - 38 G. Shi, K. Chen, Y. Wang, H. Li and C. Wang, Highly efficient synthesis of quinazoline-2, 4(1*H*, 3*H*)-diones from CO<sub>2</sub> by hydroxyl functionalized aprotic ionic liquids, *ACS Sustainable Chem. Eng.*, 2018, **6**, 5760–5765.
  - 39 R. Li, Y. Zhao, Z. Li, Y. Wu, J. Wang and Z. Liu, Choline-based ionic liquids for CO<sub>2</sub> capture and conversion, *Sci. China: Chem.*, 2019, **62**, 256–261.
  - 40 Y. Chen and T. Mu, Conversion of CO<sub>2</sub> to value-added products mediated by ionic liquids, *Green Chem.*, 2019, **21**, 2544–2574.
  - 41 Y.-B. Wang, Y.-M. Wang, W.-Z. Zhang and X.-B. Lu, Fast CO<sub>2</sub> sequestration, activation, and catalytic transformation using *N*-heterocyclic olefins, *J. Am. Chem. Soc.*, 2013, **135**, 11996–12003.
  - 42 A. Mazheika, Y. G. Wang, R. Valero, F. Viñes, F. Illas, L. M. Ghiringhelli, S. V. Levchenko and M. Scheffler, Artificial-intelligence-driven discovery of catalyst genes with application to CO<sub>2</sub> activation on semiconductor oxides, *Nat. Commun.*, 2022, **13**, 419.
  - 43 A. E. Green, J. Justen, W. Schöllkopf, A. S. Gentleman, A. Fielicke and S. R. Mackenzie, IR Signature of size-selective CO<sub>2</sub> activation on small platinum cluster anions, Pt<sup>*n*−</sup> (*n* = 4–7), *Angew. Chem., Int. Ed.*, 2018, **57**, 14822–14826.